Journal of Adhesion Science and Technology

Publication details, including instructions for authors and subscription information:
http://www.tandfonline.com/loi/tast20

Analysis of stresses in adhesive joints applicable to IC chips using symbolic manipulation and the numerical method

Tung-Hua Cheng , Ching-Huan Tseng & Ching-Hua Hung

Published online: 02 Apr 2012.

To cite this article: Tung-Hua Cheng , Ching-Huan Tseng & Ching-Hua Hung (2006) Analysis of stresses in adhesive joints applicable to IC chips using symbolic manipulation and the numerical method, Journal of Adhesion Science and Technology, 20:15, 1669-1692, DOI: 10.1163/156856106779024463

To link to this article: http://dx.doi.org/10.1163/156856106779024463

J. Adhesion Sci. Technol., Vol. 20, No. 15, pp. 1669–1692 (2006)

Also available online - www.brill.nl/jast

Analysis of stresses in adhesive joints applicable to IC chips using symbolic manipulation and the numerical method

TUNG-HUA CHENG *, CHING-HUAN TSENG and CHING-HUA HUNG

Department of Mechanical Engineering, National Chiao Tung University, Hsinchu, Taiwan 30050, R.O.C.

Received in final form 10 September 2006

Abstract—In this study, a concentrated force is applied to both adherends bonded by an adhesive under pin–pin boundary conditions. First a mathematical model is derived with governing equations and boundary conditions. These complicated, and analytically problematic, coupled equations are solved numerically using symbolic manipulation and singular value decomposition (SVD). Also discussed are the effects of major factors, including the relative thickness of adherends, joint length and the action point of the concentrated force on the peel and shear stresses in the adhesive layer. This study identifies the conditions under which the upper adherend without breakage can be fully separated from the lower adherend. Particularly, it is found that the thickness of the lower adherend should be greater than ten times that of the adhesive layer but less than one-third that of the upper adherend, the adhesive layer should be relatively thin ($h_a \leqslant 0.01$ mm), and the adhesive joint should be relatively short (thickness to length ratio $\gamma_1 \geqslant 0.08$).

Keywords: Coupled equations; adhesive joint; symbolic manipulation; singular value decomposition; peel stress; shear stress.

1. INTRODUCTION

Adhesively-bonded joints are widely used as structural elements for aerospace vehicles and automobiles. However, as the today's IC chips tend to be much thinner and smaller than the previous constructions, they often break during the IC chip pick-up process. In this process, a wafer must be affixed with an adhesive onto a blue tape before being cut into pieces (so-called IC chips) by a diamond cutter. Subsequently, a concentrated force is applied to the blue tape from which the IC chip must be separated. Strictly speaking, there are two adherends — the IC chip (upper adherend) and the blue tape (lower adherend) bonded by an adhesive in the

*To whom correspondence should be addressed. Tel.: (886-5) 631-5480; Fax: (886-5) 636-1981; e-mail: chength@nfu.edu.tw

IC chip pick-up process. Therefore, understanding the peel and shear stresses in the adhesive layer between the IC chip and the blue tape is very important for the adhesive joint in the IC chip pick-up process.

Adhesively bonded single-lap joints have been widely studied since the 1950s. One of the most widely quoted papers on stresses in adhesive joints is that of Goland and Reissner [1]. Other studies [2–9] that have used and extended the Goland–Reissner theory and compared their own results with Goland–Reissner's have treated both the adherend and adhesive materials as anisotropic, orthotropic, or isotropic using either a finite element analysis or theoretical analysis. In addition, Luo and Tong [10] applied linear and higher-order displacement theories to stress analysis of a thick adhesive and validated their results through two-dimensional finite element analysis.

Some studies have investigated the plastic behavior in adhesive joints using analytical methods; for example, a recent elastoplastic stress analysis of a single-lap joint subjected to bending moment was carried out using the finite element method [11]. Early on, Chen and Cheng [12] analyzed an adhesively-bonded single-lap joint by minimizing the functional of the variational principle of complementary energy. Subsequently, Alexandrov and Richmond [13] addressed three-dimensional, kinematically admissible velocity fields in a flat layer of an ideally rigid plastic material subjected to tension, while Mortensen and Thomsen [14] applied the multi-segment method of integration to solve the multiple-point boundary value problem.

Some researchers have investigated thermal stress in an adhesive layer subjected to temperature variation [15–18], while others have addressed cracks resulting in failure or the stress singularity in the fillet of an adhesive joint [19–21]. In addition, single-lap adhesive joints of dissimilar adherends have been subjected to external bending moments and tensile loads [22, 23], and a single-lap joint subjected to tension loading and moments induced by geometric eccentricity was studied using the finite element method [24].

Besides, some other technical studies have shown that a structure is strengthened by adhesively bonding the steel plates to the tension face of the beam [25, 26]. However, Cornell [27], who claimed that obtaining complete theoretical solutions to this problem would be very difficult, only considered a cantilever beam consisting of the same adherends. Only if the characteristic solutions of these equations have appropriately large values, his method can produce classical solutions for the differential equations.

Therefore, in this present study both adhesively-bonded adherends are subjected to a concentrated force and the peel and shear stress distributions in the adhesive layer joining the two adherends are examined. Such stress distributions are affected by geometric conditions, including the thicknesses of adherends and the length and thickness of the adhesive layer, as well as by the action point of the concentrated force. As obtaining analytical solutions is even more difficult here than in the work of Cornell [27], the model uses symbolic manipulation to solve the coupled differential equations in the Mathematica package, thereby enabling

to find complete and complicated solutions that are not limited to finding only the characteristic solutions having large values (i.e., the characteristic solutions had to have large values [27]). In this analysis, 31 constraint and boundary conditions are considered in the analytical solutions. Thus, the numerical solutions can be found by singular value decomposition (SVD) [29] employed as the basis for finding the inverse of a matrix in which the magnitude of the matrix elements varies much. Nevertheless, it is still somewhat difficult to converge and directly solve the differential equations using the numerical method.

2. MATHEMATICAL MODEL

In this model the two adherends — the upper adherend and lower adherend — are bonded by an adhesive layer with the center coinciding with the origin of the coordinate system (see Fig. 1). The thicknesses of the upper adherend, lower adherend and adhesive layer are denoted by h_1, h_2 and h_a, respectively. Their lengths are represented, respectively, by $2c$, $(L_1 + L_2)$ and $2c$. The lower adherend is subjected to a concentrated force P under the pin–pin boundary conditions.

The governing equations for this study are based on the following assumptions:

(a) The transverse displacements of both the upper adherend and the lower adherend subjected to the concentrated force P are much smaller than their dimensions, and their transverse displacements are presumed to be linear and small.

(b) Both the upper adherend and the lower adherend deform under a plane-stress condition; in other words, the plane section remains plane and the deformation of the cross-sections is correspondingly normal to the neutral surfaces.

(c) The variations in both longitudinal and transverse displacements are linear in the adhesive layer.

(d) In the adhesive layer, the stress resulting from the longitudinal force is ignored when compared with stresses in the upper adherend and lower adherend [10].

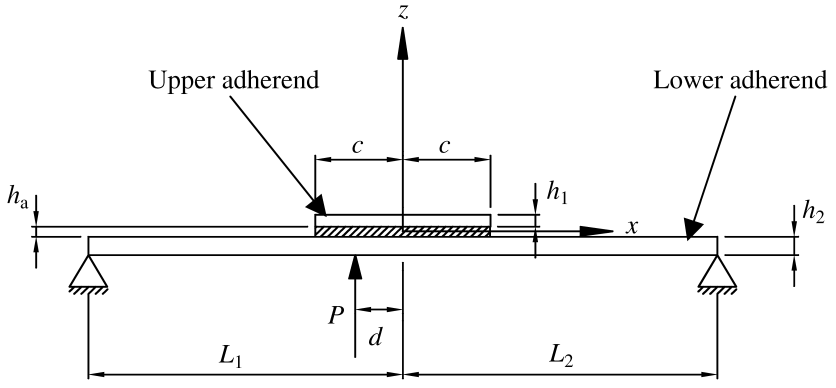

Figure 1. The sketch showing two adherends bonded by an adhesive layer.

Based on the preceding assumptions, the governing equations are derived as follows. First, the lower adherend is divided into four segments whose ranges are $-L_1 \leqslant x \leqslant -c$, $-c \leqslant x \leqslant -d$, $-d \leqslant x \leqslant c$ and $c \leqslant x \leqslant L_2$, respectively on the x-axis. Next, the upper adherend is divided into two segments whose ranges are $-c \leqslant x \leqslant -d$ and $-d \leqslant x \leqslant c$ on the x-axis. Finally, the adhesive layer is also divided into two segments, each of which has the same range as the corresponding segment in the upper adherend.

2.1. Bending moment, shear force and longitudinal force in the upper and lower adherend

The free-body diagram for the first segment ($-L_1 \leqslant x \leqslant -c$) is shown in Fig. 2, where N_{L} and F_{L} represent the longitudinal force and reaction force, respectively, of the left-end support, and the bending moment, shear force and longitudinal force of the first segment's right-hand section are denoted by M_{1x}, Q_{1x} and N_{1x}, in which the $1x$ subscript refers to the first segment of the lower adherend. According to force and moment equilibria equations, the bending moment M_{1x}, the shear force Q_{1x} and the longitudinal force N_{1x} can be derived in terms of N_{L} and F_{L} as:

$$M_{1x} = -F_{\mathrm{L}}(L_1 + x), \tag{1}$$

$$Q_{1x} = F_{\mathrm{L}} \tag{2}$$

and

$$N_{1x} = N_{\mathrm{L}}. \tag{3}$$

Similarly, in the free-body diagrams for the second, third, and fourth segments (displayed in Figs 3, 4 and 5, respectively), the bending moment, shear force, and longitudinal force of the section for the ith ($i = 2$–4) segment, denoted by M_{ix}, Q_{ix} and N_{ix}, respectively, can be written as shown below.

Specifically, the bending moment, shear force, and longitudinal force of the second segment's right-hand section ($-c \leqslant x \leqslant -d$) are as follows:

$$M_{2x} = -F_{\mathrm{L}}(L_1 + x) + \int_{-c}^{x} x\sigma_{\mathrm{a}2}\,\mathrm{d}x + \frac{h_2}{2}\int_{-c}^{x} \tau_{\mathrm{a}2}\,\mathrm{d}x, \tag{4}$$

$$Q_{2x} = F_{\mathrm{L}} - \int_{-c}^{x} \sigma_{\mathrm{a}2}\,\mathrm{d}x \tag{5}$$

and

$$N_{2x} = N_{\mathrm{L}} - \int_{-c}^{x} \tau_{\mathrm{a}2}\,\mathrm{d}x, \tag{6}$$

where $\sigma_{\mathrm{a}2}$ and $\tau_{\mathrm{a}2}$ are the peel stress and shear stress for the first segment of the adhesive layer.

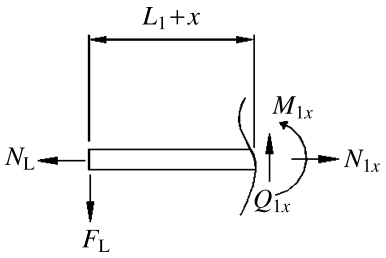

Figure 2. Free-body diagram for the first segment, $-L_1 \leqslant x \leqslant -c$, of lower adherend.

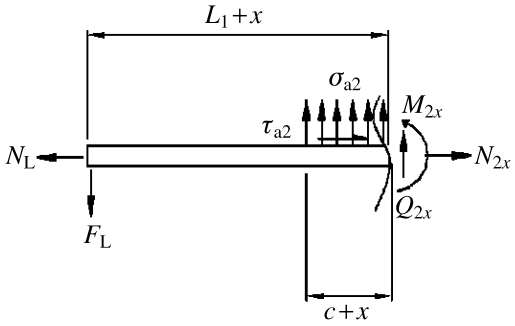

Figure 3. Free body diagram for the second segment, $-c \leqslant x \leqslant -d$, of lower adherend.

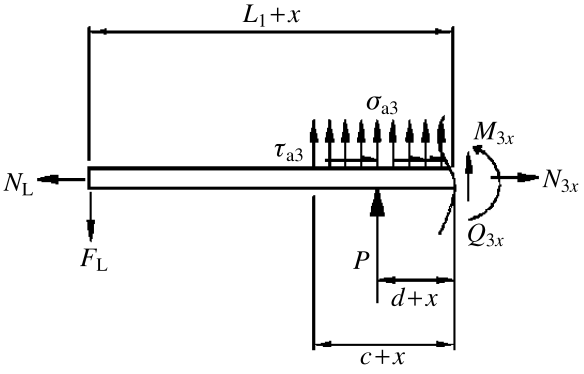

Figure 4. Free body diagram for the third segment, $-d \leqslant x \leqslant c$, of lower adherend.

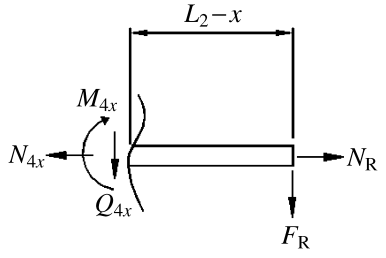

Figure 5. Free body diagram for the fourth segment, $c \leqslant x \leqslant L_2$, of lower adherend.

Similarly, the bending moment, shear force, and longitudinal force of the third segment's right-hand section ($-d \leqslant x \leqslant c$) are

$$M_{3x} = -F_{\mathrm{L}}(L_1 + x) + \int_{-c}^{x} x\sigma_{\mathrm{a3}}\,\mathrm{d}x + \frac{h_2}{2}\int_{-c}^{x} \tau_{a3}\,\mathrm{d}x + P(d + x), \tag{7}$$

$$Q_{3x} = F_{\mathrm{L}} - \int_{-c}^{x} \sigma_{\mathrm{a3}}\,\mathrm{d}x - P \tag{8}$$

and

$$N_{3x} = N_{\mathrm{L}} - \int_{-c}^{x} \tau_{\mathrm{a3}}\,\mathrm{d}x, \tag{9}$$

where σ_{a3} and τ_{a3} are the peel stress and shear stress for the second segment of the adhesive layer.

Lastly, the bending moment, shear force, and longitudinal force of the fourth segment's left-hand section ($c \leqslant x \leqslant L_2$) are

$$M_{4x} = -F_{\mathrm{R}}(L_2 - x) = (F_{\mathrm{L}} - P)(L_2 - x), \tag{10}$$

$$Q_{4x} = -F_{\mathrm{R}} = (F_{\mathrm{L}} - P) \tag{11}$$

and

$$N_{4x} = N_{\mathrm{R}} = N_{\mathrm{L}}. \tag{12}$$

The upper adherend, whose range is $-c \leqslant x \leqslant c$ on the x-axis, must be divided into two segments whose ranges are $-c \leqslant x \leqslant -d$ and $-d \leqslant x \leqslant c$, respectively. Free-body diagrams of these two segments are presented in Figs 6 and 7. The bending moment, shear force and longitudinal force of the right section of the ith segment of the upper adherend, denoted as M_i, Q_i and N_i, respectively, are as follows:

$$M_i = \int_{-c}^{x} x\sigma_{\mathrm{a}i}\,\mathrm{d}x + \frac{h_1}{2}\int_{-c}^{x} \tau_{\mathrm{a}i}\,\mathrm{d}x, \quad i = 2 \text{ or } 3, \tag{13}$$

$$Q_i = \int_{-c}^{x} \sigma_{\mathrm{a}i}\,\mathrm{d}x, \quad i = 2 \text{ or } 3, \tag{14}$$

$$N_i = \int_{-c}^{x} \tau_{\mathrm{a}i}\,\mathrm{d}x, \quad i = 2 \text{ or } 3. \tag{15}$$

When $i = 2$, the range of the upper adherend is $-c \leqslant x \leqslant -d$ (i.e., the first segment of the upper adherend). However, when $i = 3$, the range of the upper adherend is $-d \leqslant x \leqslant c$ (i.e., the second segment of the upper adherend).

2.2. Relationship between displacement and stress

When the range of the adhesive layer for bonding the upper adherend to the lower adherend is $-c \leqslant x \leqslant c$, the equations adopted from Ref. [4] are simplified by the

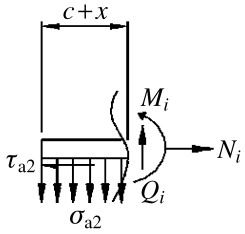

Figure 6. Free body diagram for the first segment, $-c \leqslant x \leqslant -d$, of upper adherend.

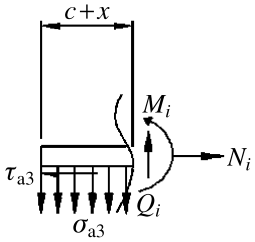

Figure 7. Free body diagram for the second segment, $-d \leqslant x \leqslant c$, of upper adherend.

small strain (i.e. the slope of the beam = 0) and are expressed as follows:

$$\sigma_{ai} = E_a \frac{(w_i - w_{ix})}{h_a}, \quad i = 2 \text{ or } 3, \tag{16}$$

$$\tau_{ai} = \frac{G_a(u_i(h_a/2) - u_{ix}(-h_a/2))}{h_a}, \quad i = 2 \text{ or } 3, \tag{17}$$

where u_i and w_i represent longitudinal and transverse displacements when $i = 2$ represents the first segment ($-c \leqslant x \leqslant -d$) of the upper adherend and $i = 3$ represents its second segment ($-d \leqslant x \leqslant c$). In equations (16) and (17), when $i = 2$, transverse and longitudinal displacements for the second segment of the lower adherend are denoted by w_{2x}, u_{2x}, and when $i = 3$, those for the third segment of the lower adherend are denoted by w_{3x}, u_{3x}. These variables, which are either functions of both x and z or only a function of x, are expressed as $u_i = u_i(x, z)$, $u_{ix} = u_{ix}(x, z)$, $w_i = w_i(x)$ and $w_{ix} = w_{ix}(x)$ ($i = 2$ or 3). The longitudinal displacement $u_i(h_a/2)$ of the upper adherend and the longitudinal displacement $u_{ix}(-h_a/2)$ of the lower adherend are then represented as a function of x and are expressed as either $z = h_a/2$ or $z = -h_a/2$. The symbols G_a, E_a and h_a, respectively, denote the shear modulus, Young's modulus and the thickness of the adhesive layer.

2.3. Relationships among displacement, longitudinal force and bending moment

Following the beam theory, the transverse displacements w_i of the upper adherend and w_{ix} of the lower adherend are written as shown below:

$$\frac{\mathrm{d}^2 w_{ix}}{\mathrm{d}x^2} = \frac{12M_{ix}}{E_2^* h_2^3}, \quad i = 1 \text{ or } 4, \tag{18}$$

$$\frac{\mathrm{d}^2 w_i}{\mathrm{d}x^2} = \frac{12M_i}{E_1^* h_1^3}, \quad i = 2 \text{ or } 3, \tag{19}$$

where $E_2^* = \bar{E}_2$, $E_1^* = \bar{E}_1$ represent Young's modulus of the upper adherend and of the lower adherend in plane stress.

The longitudinal displacements u_i, of the upper adherend, and u_{ix}, of the lower adherend, can then be written as follows:

$$\frac{\mathrm{d}u_{ix}}{\mathrm{d}x} = \frac{1}{E_2^*}\left(\frac{N_{ix}}{h_2} + \frac{12M_{ix}z''}{h_2^3}\right), \quad i = 1 \text{ or } 4, \tag{20}$$

$$\frac{\mathrm{d}u_i}{\mathrm{d}x} = \frac{1}{E_1^*}\left(\frac{N_i}{h_1} + \frac{12M_i z'}{h_1^3}\right), \quad i = 2 \text{ or } 3, \tag{21}$$

where $z'' = z + (h_2 + h_\mathrm{a})/2$ and $z' = z - (h_1 + h_\mathrm{a})/2$.

To obtain the longitudinal displacements, transverse displacements, and slopes of the first and fourth segments in the lower adherend, equations (1)–(3) and (10)–(12) are substituted into equations (18) and (20) which are integrated over x to produce the following expressions:

$$\frac{\mathrm{d}w_{1x}}{\mathrm{d}x} = -\frac{6F_\mathrm{L}(2L_1 x + x^2)}{E_2^* h_2^3} + c_{11}, \quad -L_1 \leqslant x \leqslant -c, \tag{22}$$

$$w_{1x} = -\frac{2F_\mathrm{L}(3L_1 x^2 + x^3)}{E_2^* h_2^3} + c_{11}x + c_{12}, \quad -L_1 \leqslant x \leqslant -c, \tag{23}$$

$$u_{1x} = \frac{1}{E_2^*}\left(\frac{N_\mathrm{L}}{h_2}x - \frac{6F_\mathrm{L}(2L_1 x + x^2)z''}{h_2^3}\right) + c_{13}, \quad -L_1 \leqslant x \leqslant -c, \tag{24}$$

$$\frac{\mathrm{d}w_{4x}}{\mathrm{d}x} = -\frac{6(P - F_\mathrm{L})(2L_2 x - x^2)}{E_2^* h_2^3} + c_{41}, \quad c \leqslant x \leqslant L_2, \tag{25}$$

$$w_{4x} = -\frac{2(P - F_\mathrm{L})(3L_2 x^2 - x^3)}{E_2^* h_2^3} + c_{41}x + c_{42}, \quad c \leqslant x \leqslant L_2, \tag{26}$$

$$u_{4x} = \frac{1}{E_2^*}\left(\frac{N_\mathrm{L}}{h_2}x - \frac{6(P - F_\mathrm{L})(2L_2 x - x^2)z''}{h_2^3}\right) + c_{43}, \quad c \leqslant x \leqslant L_2, \tag{27}$$

where c_{ik} are constants. The subscripts i and k of c_{ik} represent the ith segment of the lower adherend and the index of the constants.

Substituting M_{ix} and N_{ix} from equations (18)–(21) into equations (4), (6), (7) and (9), where $\sigma_{\mathrm{a}2}$, $\tau_{\mathrm{a}2}$, $\sigma_{\mathrm{a}3}$ and $\tau_{\mathrm{a}3}$ are replaced by equations (16) and (17), gives

the following equations for the second and third segments of the lower adherend:

$$\frac{\mathrm{d}^4 w_{ix}}{\mathrm{d}x^4} = \frac{12}{E_2^* h_2^3}\left\{\frac{E_\mathrm{a}}{h_\mathrm{a}}(w_i - w_{ix}) + \frac{E_2^* h_2^2}{2}\left(-z''\frac{\mathrm{d}^4 w_{ix}}{\mathrm{d}x^4} - \frac{\mathrm{d}^3 u_{ix}}{\mathrm{d}x^3}\right)\right\}, \quad i = 2 \text{ or } 3, \tag{28}$$

$$\frac{\mathrm{d}^2 u_{ix}}{\mathrm{d}x^2} = \frac{12}{E_2^* h_2}\left[-\frac{G_\mathrm{a}}{h_\mathrm{a}}\left(u_i\left(\frac{h_\mathrm{a}}{2}\right) - u_{ix}\left(-\frac{h_\mathrm{a}}{2}\right)\right)\right] - z''\frac{\mathrm{d}^3 w_{ix}}{\mathrm{d}x^3}, \quad i = 2 \text{ or } 3. \tag{29}$$

Using the previous procedure, the formulas for the first and second segments of the upper adherend can be obtained as follows:

$$\frac{\mathrm{d}^4 w_i}{\mathrm{d}x^4} = \frac{12}{E_1^* h_1^3}\left\{\frac{E_\mathrm{a}}{h_\mathrm{a}}(w_i - w_{ix}) + \frac{E_1^* h_1^2}{2}\left(z'\frac{\mathrm{d}^4 w_i}{\mathrm{d}x^4} + \frac{\mathrm{d}^3 u_i}{\mathrm{d}x^3}\right)\right\}, \quad i = 2 \text{ or } 3, \tag{30}$$

$$\frac{\mathrm{d}^2 u_i}{\mathrm{d}x^2} = \frac{12}{E_1^* h_1}\left[-\frac{G_\mathrm{a}}{h_\mathrm{a}}\left(u_i\left(\frac{h_\mathrm{a}}{2}\right) - u_{ix}\left(-\frac{h_\mathrm{a}}{2}\right)\right)\right] - z'\frac{\mathrm{d}^3 w_i}{\mathrm{d}x^3}, \quad i = 2 \text{ or } 3. \tag{31}$$

2.4. Non-dimensionalization

To regulate the magnitude of some parameters and illustrate clearly the detailed relationships among them, the parameters are non-dimensionalized and are listed in Table 1. For the first and fourth segments of the lower adherend, equations (22)–(27) can be non-dimensionalized and rearranged as follows:

$$\frac{\mathrm{d}w_{1x}}{\mathrm{d}x} = -\frac{6\tilde{F}_\mathrm{L}(2L_1 x + x^2)}{E_2 h_2^3} + c_{11}, \quad -L_1 \leqslant x \leqslant -c, \tag{32}$$

$$w_{1x} = -\frac{2\tilde{F}_\mathrm{L}(3L_1 x^2 + x^3)}{E_2 h_2^3} + c_{11}x + c_{12}, \quad -L_1 \leqslant x \leqslant -c, \tag{33}$$

$$u_{1x} = \frac{1}{E_2}\left(\frac{\tilde{N}_\mathrm{L}}{h_2}x - \frac{6\tilde{F}_\mathrm{L}(2L_1 x + x^2)z''}{h_2^3}\right) + c_{13}, \quad -L_1 \leqslant x \leqslant -c, \tag{34}$$

$$\frac{\mathrm{d}w_{4x}}{\mathrm{d}x} = -\frac{6(\tilde{P} - \tilde{F}_\mathrm{L})(2L_2 x - x^2)}{E_2 h_2^3} + c_{41}, \quad c \leqslant x \leqslant L_2, \tag{35}$$

$$w_{4x} = -\frac{2(\tilde{P} - \tilde{F}_\mathrm{L})(3L_2 x^2 - x^3)}{E_2 h_2^3} + c_{41}x + c_{42}, \quad c \leqslant x \leqslant L_2, \tag{36}$$

$$u_{4x} = \frac{1}{E_2}\left(\frac{\tilde{N}_\mathrm{L}}{h_2}x - \frac{6(\tilde{P} - \tilde{F}_\mathrm{L})(2L_2 x - x^2)z''}{h_2^3}\right) + c_{43}, \quad c \leqslant x \leqslant L_2, \tag{37}$$

where

$$E_1 = \frac{E_1^*}{G_\mathrm{a}}, \quad E_0 = \frac{E_a}{G_\mathrm{a}}, \quad E_2 = \frac{E_2^*}{G_\mathrm{a}}, \quad \tilde{N}_\mathrm{L} = \frac{N_\mathrm{L}}{G_\mathrm{a}}, \quad \tilde{F}_\mathrm{L} = \frac{F_\mathrm{L}}{G_\mathrm{a}} \quad \text{and} \quad \tilde{P} = \frac{P}{G_\mathrm{a}}.$$

Table 1.
The non-dimensional terms and equations for upper adherend, adhesive layer and lower adherend

Non-dimensional terms for upper adherend	Equation	Non-dimensional terms for lower adherend	Equation	Non-dimensional terms for adhesive layer	Equation
Thickness ratio	$\beta_1 = \frac{h_1}{h_a}$	Thickness ratio	$\beta_2 = \frac{h_2}{h_a}$	Peel stress	$\overline{\sigma}_{ai} = \frac{2c\sigma_{ai}}{P}$
Thickness to length ratio	$\gamma_1 = \frac{h_1}{2c}$	Thickness to length ratio	$\gamma_2 = \frac{h_2}{2c}$	Shear stress	$\overline{\tau}_{ai} = \frac{2c\tau_{ai}}{P}$
Elastic modulus	$E_1 = \frac{E_1^*}{G_a}$	Elastic modulus	$E_2 = \frac{E_2^*}{G_a}$	Elastic modulus	$E_0 = \frac{E_a}{G_a}$
Shear force	$\overline{Q}_i = \frac{Q_i}{P}$	Shear force	$\overline{Q}_{ix} = \frac{Q_{ix}}{P}$	x-axis	$\bar{x} = \frac{x}{c}$
Moment	$\overline{M}_i = \frac{M_i}{2Pc}$	Moment	$\overline{M}_{ix} = \frac{M_{ix}}{2Pc}$		
Longitudinal force	$\overline{N}_i = \frac{N_i}{P}$	Longitudinal force	$\overline{N}_{ix} = \frac{N_{ix}}{P}$		

Equations (28)–(31) can then be rewritten in the matrix form as:

$$\begin{bmatrix} D^2 - \frac{1}{E_1\beta_1 h_a^2} & \frac{1}{E_1\beta_1 h_a^2} & -\frac{\beta_1 h_a}{2}D^3 - \frac{1}{E_1\beta_1 h_a}D & 0 \\ \frac{1}{E_2\beta_2 h_a^2} & D^2 - \frac{1}{E_2\beta_2 h_a^2} & 0 & \frac{\beta_2 h_a}{2}D^3 + \frac{1}{E_2\beta_2 h_a}D \\ \frac{6}{\beta_1 h_a}D^3 & 0 & -4D^4 - \frac{1}{h_a d_1} & \frac{1}{h_a d_1} \\ 0 & \frac{-6}{\beta_2 h_a}D^3 & \frac{1}{h_a d_2} & -4D^4 - \frac{1}{h_a d_2} \end{bmatrix} \begin{bmatrix} \tilde{u}_i \\ \tilde{u}_{ix} \\ w_i \\ w_{ix} \end{bmatrix} = [\mathbf{A}_D][u] = 0, \tag{38}$$

where $\tilde{u}_i = u_i(h_a/2)$, $\tilde{u}_{ix} = u_{ix}(-h_a/2)$ and $D = \frac{d}{dx}$, i may be either 2 or 3, the non-dimensional terms are $\beta_1 = h_1/h_a$ and $\beta_2 = h_2/h_a$, and other parameters are

$$d_1 = \frac{h_1^3 E_1^*}{12E_a}, \quad d_2 = \frac{h_2^3 E_2^*}{12E_a}.$$

The characteristic equation, $\det|\mathbf{A}_D| = 0$, of coupled differential equation (38) can then be derived as follows:

$$\begin{aligned} &\left[D^{12} - \left(\frac{4}{\beta_1 E_1 h_a^2} + \frac{4}{\beta_2 E_2 h_a^2}\right)D^{10} + \left(\frac{1}{d_1 h_a}\frac{1}{d_2 h_a}\right)D^8 \right. \\ &\quad - \left(\frac{1}{\beta_1 d_1 E_1 h_a^3} + \frac{4}{\beta_1 d_2 E_1 h_a^3} + \frac{3\beta_2}{\beta_1^2 d_2 E_1 h_a^3} \right. \\ &\qquad \left. \left. + \frac{3\beta_1}{\beta_2^2 d_1 E_2 h_a^3} + \frac{4}{\beta_2 d_1 E_2 h_a^3} + \frac{1}{\beta_2 d_2 E_2 h_a^3}\right)D^6\right] \\ &\quad \times \{\tilde{u}_i, w_i, \tilde{u}_{ix}, w_{ix}\} = 0, \quad i = 2 \text{ or } 3. \end{aligned} \tag{39}$$

Assuming that α and $\pm\alpha_{11} \pm i\alpha_{12}$ are the roots of the characteristic equation (39), the transverse displacements w_i of the upper adherend are written in the following

form:

$$w_i = c_{i0} + c_{i1}x + c_{i2}x^2 + c_{i3}x^3 + c_{i4}x^4 + c_{i5}x^5 + c_{i6}\overline{Ch} + c_{i7}\overline{Sh} + \overline{Ch}_1(c_{i8}\overline{C} + c_{i9}\overline{S}) + \overline{Sh}_1(c_{i10}\overline{C} + c_{i11}\overline{S}), \quad i = 2 \text{ or } 3, \tag{40}$$

where $\overline{Ch} = \cosh(\alpha x)$, $\overline{Sh} = \sinh(\alpha x)$, $\overline{Ch}_1 = \cosh(\alpha_{11}x)$, $\overline{Sh}_1 = \sinh(\alpha_{11}x)$, and the unknown constants are c_{ij}, $i = 2$ or 3, $j = 0$–11, $\overline{C} = \cos(\alpha_{12}x)$ and $\overline{S} = \sin(\alpha_{12}x)$.

As the complete solutions of the model are extremely complex, this study employed Mathematica's symbolic manipulation to solve $\tilde{u}_i$, $\tilde{u}_{ix}$, w_{ix}, $\frac{\mathrm{d}w_{ix}}{\mathrm{d}x}$ and $\frac{\mathrm{d}w_i}{\mathrm{d}x}$ in terms of c_{ij}, $\overline{S}$, $\overline{C}$, $\overline{Ch}$, $\overline{Sh}$, $\overline{Ch}_1$ and $\overline{Sh}_1$. To prove whether these analytical solutions are correct, they are once again substituted into the system differential equation (39), which shows c_{i4} and c_{i5} to be equal to zero.

The analytical solutions $\tilde{u}_i$, $\tilde{u}_{ix}$, w_i and w_{ix}, which are substituted into equations (16) and (17), and the adhesive layer's non-dimensional peel and shear stresses $\overline{\sigma}_{ai} = 2c\sigma_{ai}/P$ and $\overline{\tau}_{ai} = 2c\tau_{ai}/P$ (listed in Table 1) are then formulated in terms of c_{ij}, $\overline{S}$, $\overline{C}$, $\overline{Ch}$, $\overline{Sh}$, $\overline{Ch}_1$ and $\overline{Sh}_1$ (i.e., analytical stress solutions, $\overline{\sigma}_{ai}$ and $\overline{\tau}_{ai}$).

The analytical stress solutions, $\overline{\sigma}_{ai}$ and $\overline{\tau}_{ai}$, are substituted into equations (4)–(9), (13)–(15). The shear force $\overline{Q}_i = Q_i/P$, the bending moment $\overline{M}_i = M_i/(2Pc)$ and the longitudinal force $\overline{N}_i = N_i/P$ for the upper adherend, as well as the shear force $\overline{Q}_{ix} = Q_{ix}/P$, the bending moment $\overline{M}_{ix} = M_{ix}/(2Pc)$ and the longitudinal force $\overline{N}_{ix} = N_{ix}/P$ for the lower adherend (all listed in Table 1) are also expressed in terms of c_{ij}, $\overline{S}$, $\overline{C}$, $\overline{Ch}$, $\overline{Sh}$, $\overline{Ch}_1$ and $\overline{Sh}_1$.

For the first and fourth segments, equations (1)–(3), (10)–(12) are rewritten and non-dimensionalized. The resulting non-dimensional bending moment, shear force and longitudinal force ($\overline{M}_{1x}$, $\overline{Q}_{1x}$, $\overline{N}_{1x}$, $\overline{M}_{4x}$, $\overline{Q}_{4x}$ and $\overline{N}_{4x}$), are formulated as shown below:

$$\overline{M}_{1x} = \frac{M_{1x}}{2Pc} = -\frac{F_{\mathrm{L}}}{2Pc}(L_1 + x) = -\frac{\tilde{F}_{\mathrm{L}}}{2\tilde{P}c}(L_1 + x), \tag{41}$$

$$\overline{Q}_{1x} = \frac{Q_{1x}}{P} = \frac{F_{\mathrm{L}}}{P} = \frac{\tilde{F}_{\mathrm{L}}}{\tilde{P}}, \tag{42}$$

$$\overline{N}_{1x} = \frac{N_{1x}}{P} = \frac{N_{\mathrm{L}}}{P} = \frac{\tilde{N}_{\mathrm{L}}}{\tilde{P}}, \tag{43}$$

$$\begin{aligned}\overline{M}_{4x} &= \frac{M_{4x}}{2Pc} = -\frac{F_{\mathrm{R}}}{2Pc}(L_2 - x) \\ &= \frac{(F_{\mathrm{L}} - P)}{2Pc}(L_2 - x) = \frac{(\tilde{F}_{\mathrm{L}} - \tilde{P})}{2\tilde{P}c}(L_2 - x),\end{aligned} \tag{44}$$

$$\overline{Q}_{4x} = \frac{Q_{4x}}{P} = -\frac{F_{\mathrm{R}}}{P} = \frac{F_{\mathrm{L}} - P}{P} = \frac{\tilde{F}_{\mathrm{L}} - \tilde{P}}{\tilde{P}}, \tag{45}$$

$$\overline{N}_{4x} = \frac{N_{4x}}{P} = \frac{N_{\mathrm{R}}}{P} = \frac{N_{\mathrm{L}}}{P} = \frac{\tilde{N}_{\mathrm{L}}}{\tilde{P}}. \tag{46}$$

3. CONSTRAINT AND BOUNDARY CONDITIONS

The constraint and boundary conditions for this study, shown in Fig. 1, can be identified and described in the following manner.

At the left-end pin support ($x = -L_1$) of the lower adherend, there are two boundary conditions, i.e., zero transverse displacement and zero longitudinal displacement of the lower adherend. At $x = -c$, there are eight constraint conditions, six of which are continuity conditions for the lower adherend. That is, at junction point ($x = -c$) between the first and second segments of the lower adherend, both segments must have the same values of transverse displacement, slope, bending moment, shear force, longitudinal force and longitudinal displacement. The other two conditions at $x = -c$ are that both the bending moment and longitudinal force of the upper adherend must be equal to zero.

At junction point ($x = -d$) between the second and third segments, there are 11 conditions, 8 of which are continuity conditions. First, in both upper and lower adherends, both segments must again have the same values of transverse displacement, slope, bending moment, and longitudinal displacement. Three other conditions are written as follows: (i) the total shear force in the left neighborhood of the junction point ($x^- = -d^-$) is $\tilde{F}_{\mathrm{L}}/\tilde{P}$, (ii) the total shear force in the right neighborhood of the junction point ($x = -d^+$) is $(\tilde{F}_{\mathrm{L}} - \tilde{P})/\tilde{P}$ and (iii) the total longitudinal force has the same value at junction point ($x = -d$) for both second and third segments.

The model also is subjected to eight constraint conditions at $x = c$. At the junction point ($x = c$) between the third and fourth segments of the lower adherend, both segments must have the same values of transverse displacement, slope, bending moment, shear force, longitudinal force and longitudinal displacement. In addition, the bending moment and longitudinal force of the upper adherend must be equal to zero.

At the right-end pin support ($x = L_2$) of the lower adherend, there are again two boundary conditions, i.e., the transverse displacement and longitudinal displacement for the lower adherend must be zero.

Overall, the number of boundary and constraint conditions totals 31, equal to the number of unknown constants. The unknown constants include c_{ij}, $c_{\mathrm{a}i1}$, $c_{\mathrm{a}i2}$, c_{1k}, c_{4k} and N_{L}, where subscript i is equal to 2 or 3, k ranges from 1 to 3, and j ranges from 1 to 12, but c_{i4} and c_{i5} (found in the preceding descriptions) equal zero. $c_{\mathrm{a}i1}$ and $c_{\mathrm{a}i2}$ are the unknown constants of the longitudinal displacements and result from substituting the analytical solutions $\tilde{u}_i$, $\tilde{u}_{ix}$, w_i and w_{ix} into the integrated equations (29) and (31).

Imposing 31 constraint and boundary equations on the analytical solutions through symbolic manipulation produces 31 system equations expressed in the following matrix form.

$$[\mathbf{A}][\mathbf{C}] = [\mathbf{B}] \tag{47}$$

where matrix [**A**] has 31 rows and 31 columns, denoted by $[\mathbf{A}]_{31\times31}$, and matrices [**B**] and [**C**] have 31 rows and 1 column, denoted by $[\mathbf{B}]_{31\times1}$ and $[\mathbf{C}]_{31\times1}$, respectively. The elements in matrix $[\mathbf{C}]_{31\times1}$ consist of 31 unknown constants, c_{ij}, c_{ai1}, c_{ai2}, c_{1k}, c_{4k} and N_{L}.

The matrix $[\mathbf{C}]_{31\times1}$ is solved using Mathematica's SVD algorithm because matrix [**A**] has a greater variation in the magnitude of the matrix elements. If one eigenvalue in the characteristic equation (39) is large, some elements of matrix [**A**] that involve $\overline{Sh}$, $\overline{Ch}$, $\overline{Sh}_1$ and $\overline{Ch}_1$ become much larger. However, the magnitude of those elements in matrix [**A**] that do not involve $\overline{Sh}$, $\overline{Ch}$, $\overline{Sh}_1$ and $\overline{Ch}_1$ is much smaller. Thus, there is a discrepancy in the magnitude of matrix [**A**] elements exceeding by exponential order of 10s. In addition, because of computer truncation errors, the inverse of matrix [**A**] cannot be obtained by the adjoint method. Therefore, matrix $[\mathbf{C}]_{31\times1}$ is solved by SVD algorithm and the non-dimensional peel stress and shear stress in the adhesive layer can be obtained by substituting matrix $[\mathbf{C}]_{31\times1}$ into the expressions $\overline{\sigma}_{ai}$ and $\overline{\tau}_{ai}$.

4. RESULTS AND DISCUSSION

Figure 8 shows the analytical solutions of this model employed to solve the problem proposed by Cornell [27], using the following values: $h_1 = 0.04$ inch (1.016 mm), $h_2 = 0.25$ inch (6.35 mm) and $h_{\mathrm{a}} = 0.1$ inch (2.54 mm), 0.01 inch (0.254 mm),

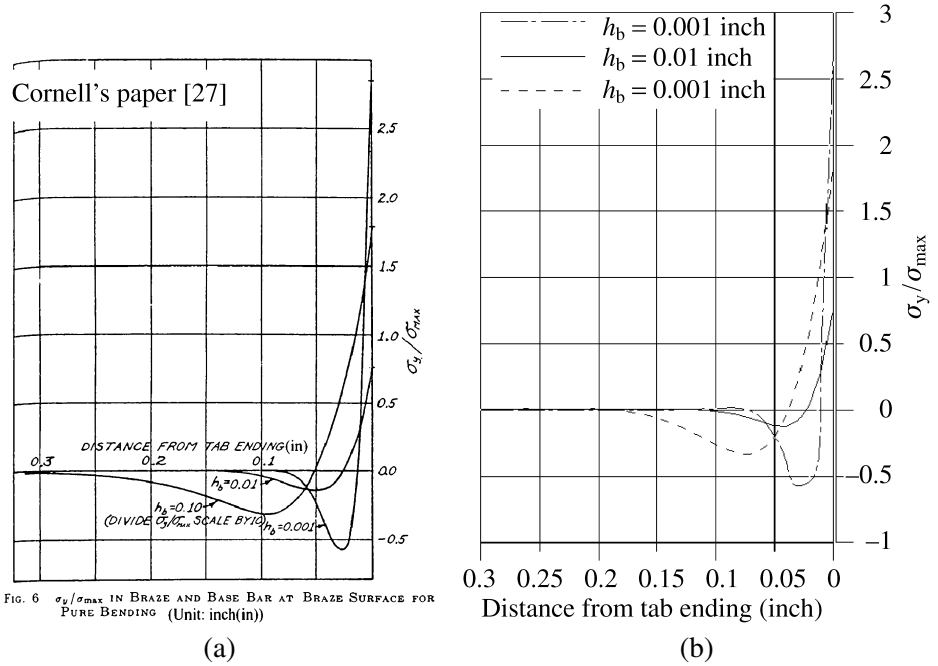

Figure 8. Comparison of the results between Fig. 6 of Ref. [27] (a) and the present study (b).

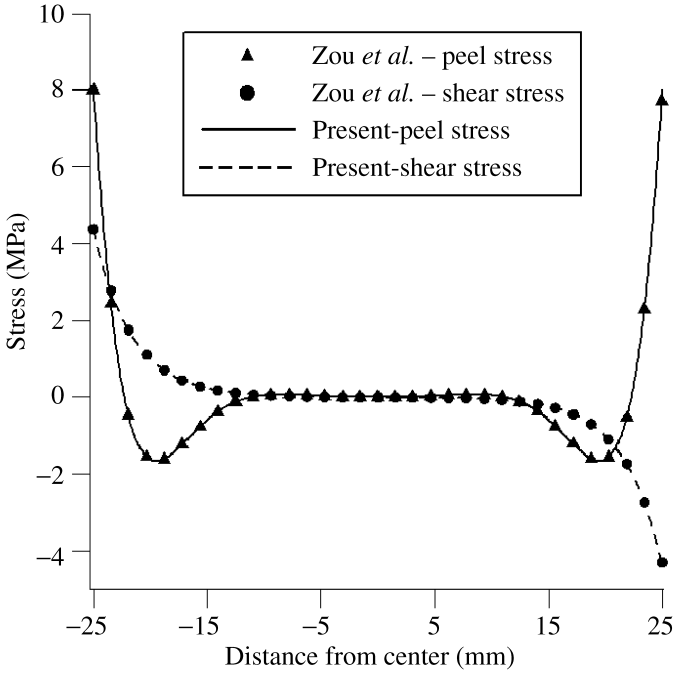

Figure 9. Comparison of the results between Fig. 5 of Ref. [28] and the present study.

and 0.001 inch (0.0254 mm). Because Cornell's Fig. 6 has used inch (in) as length units, Fig. 8 here also uses inch as length unit. All figures, except Fig. 8, use mm as length unit. It should be noted that the symbol h_a in this study is synonymous with Cornell's h_b and the profiles of Fig. 8 are nearly consistent with those of Cornell's Fig. 6. The numerical results obtained by employing the analytical solutions to solve the problem in Zou *et al.* [28] are shown in Fig. 9. These data are almost consistent with those of Fig. 5 in Ref. [28], except that for this study, the maximum shear stress is 4.38, while in Ref. [28] it is 4.30 (MPa).

The values $E_1 = 6.0$, $E_2 = 6.0$, $E_0 = 2.75$, $\tilde{P} = 1$ and $d = 0$ are used as follows. The symbols E_1, E_2, and E_0 (listed in Table 1) represent the ratios of the elastic modulus of the upper adherend, lower adherend and adhesive layer, respectively, to the shear modulus of the adhesive layer. The symbol d represents the distance from the center of the adhesive layer to the action point of the force.

4.1. Case 1: Upper adherend (h_1) and lower adherend (h_2) with the same thickness

Figure 10 shows distributions of the non-dimensional peel stress and shear stress in the adhesive layer, whose thickness is $h_a = 0.01$ mm. The thickness ratios $\beta_1 = h_1/h_a = 10$ and $\beta_2 = h_2/h_a = 10$ are defined as the thickness of the upper adherend and lower adherend respectively relative to the adhesive layer's thickness. $\bar{x} = x/c$ is both the normalized axis and the non-dimensional term of the adhesive layer, where $-1 \leqslant \bar{x} \leqslant 1$. The thickness to length ratio $\gamma = \gamma_1 = \gamma_2 = h/(2c)$ is

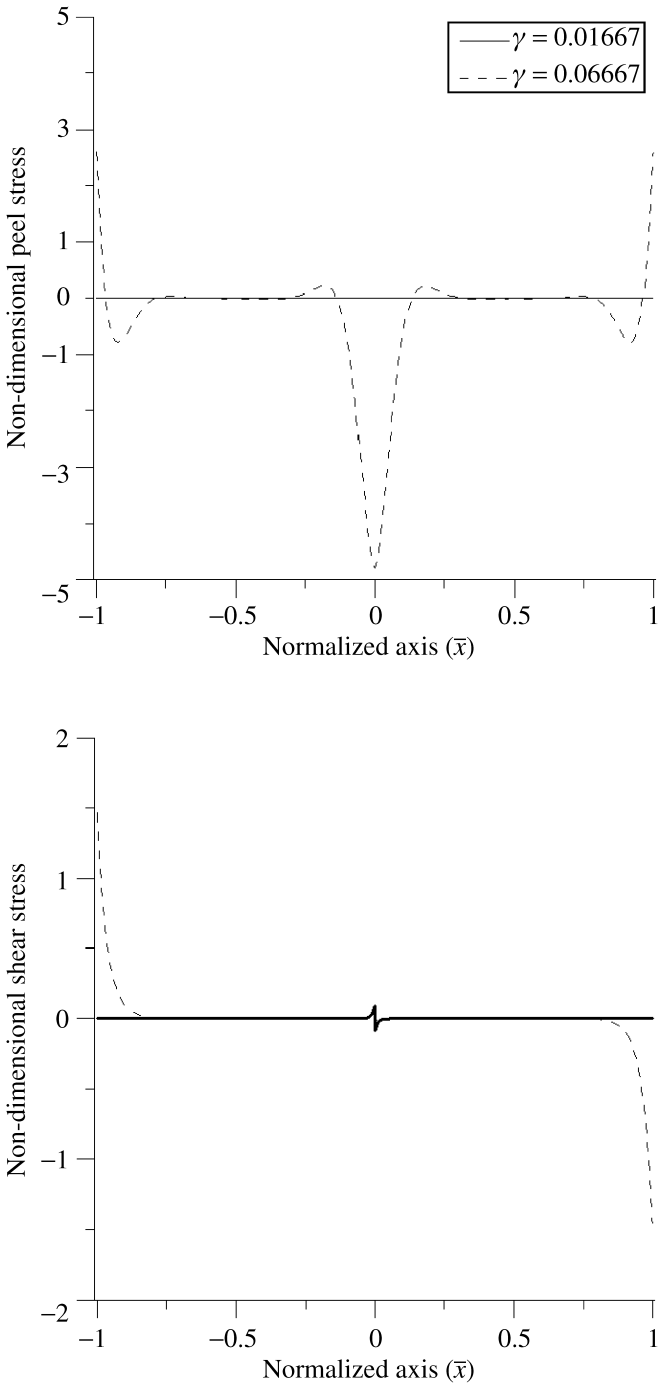

Figure 10. Non-dimensional peel and shear stresses distributions in the adhesive layer ($\bar{x} = x/c$) for the thickness to length ratio $\gamma = \gamma_1 = \gamma_2$ with the same thickness of both adherends $\beta_1 = \beta_2 = 10$ and $h_a = 0.01$ mm.

the ratio of the thickness $h = h_1 = h_2$ of the upper adherend to the length ($2c$) of the adhesive layer: $\gamma = 0.01667$ and $\gamma = 0.06667$ are used in this case. Moreover, when $\gamma = 0.01667$, the length of the adhesive layer is four times that when $\gamma = 0.06667$. Thus, the non-dimensional peel and shear stress distributions for an adhesive layer when $\gamma = 0.01667$ are different from those when $\gamma = 0.06667$. As the thickness to length ratio decreases, $\gamma = 0.06667$ to $\gamma = 0.01667$, the non-dimensional peel and shear stresses in the adhesive layer become slightly less than 0.1.

Figure 10 also illustrates that the non-dimensional maximum peel and shear stresses may occur either in the center or at the ends of the adhesive layer. Therefore, the values and positions of the non-dimensional maximum peel and shear stresses are the focus of the following paragraphs.

For the adhesive layer, as shown in Fig. 11, the non-dimensional peel stress occurs either in the center ($\bar{x} = 0$) or at the ends ($\bar{x} = \pm 1$), and the non-dimensional shear stress occurs at the ends versus the thickness to length ratio γ. As γ becomes larger, i.e., the length ($2c$) of the adhesive layer becomes smaller in the same thickness ratios $\beta = \beta_1 = \beta_2$, the peel stress in the center ($\bar{x} = 0$) is at first positive and smaller (i.e., tensile stress) but then becomes larger and then negative and even larger (i.e., compressive stress). As also shown in Fig. 11, the different thickness ratios $\beta = h/h_a$ produce the same results, $\beta = \beta_1 = \beta_2 = 10$, 20, or 30, meaning that the thickness of the upper adherend, as well as of the lower adherend, can be 10, 20, or 30 times that of the adhesive layer. Thus, if both the upper adherend and lower adherend become thinner (i.e., β decreases from 30 to 10), the peel stress in the center becomes even larger as the thickness to length ratio γ increases. Moreover, since the maximum peel stress is always located either in the center ($\bar{x} = 0$) or at the ends ($\bar{x} = 1$), as the thickness to length ratio γ gradually becomes larger, the location of the maximum peel stresses in the adhesive layer changes from the ends to the center (see Fig. 11).

4.2. Case 2: Upper adherend (h_1) and lower adherend (h_2) with different thicknesses

As Fig. 12a shows, in this case, the thickness of the upper adherend is three times that of the lower adherend, meaning that the thickness of the upper adherend in Fig. 12a is three times that in Fig. 10, even though the two figures have the same conditions otherwise. For $\gamma_1 = 0.05$ and $\gamma_2 = \frac{1}{3}\gamma_1 = 0.01667$ in Fig. 12a, the non-dimensional peel stress and shear stress distributions are very similar to those in Fig. 10 ($\gamma = 0.01667$). However, for $\gamma_1 = 0.2$ and $\gamma_2 = 0.06667$, the non-dimensional peel stress in Fig. 12a, in total contrast to the larger compressive peel stress in the center in Fig. 10 ($\gamma = 0.06667$), vanishes in the center of the adhesive layer. In Fig. 12a, the maximum peel stress at the ends is about one-and-a-quarter times that in Fig. 10, while the maximum shear stress at the ends in Fig. 12a is about 1.5, which is close to that in Fig. 10.

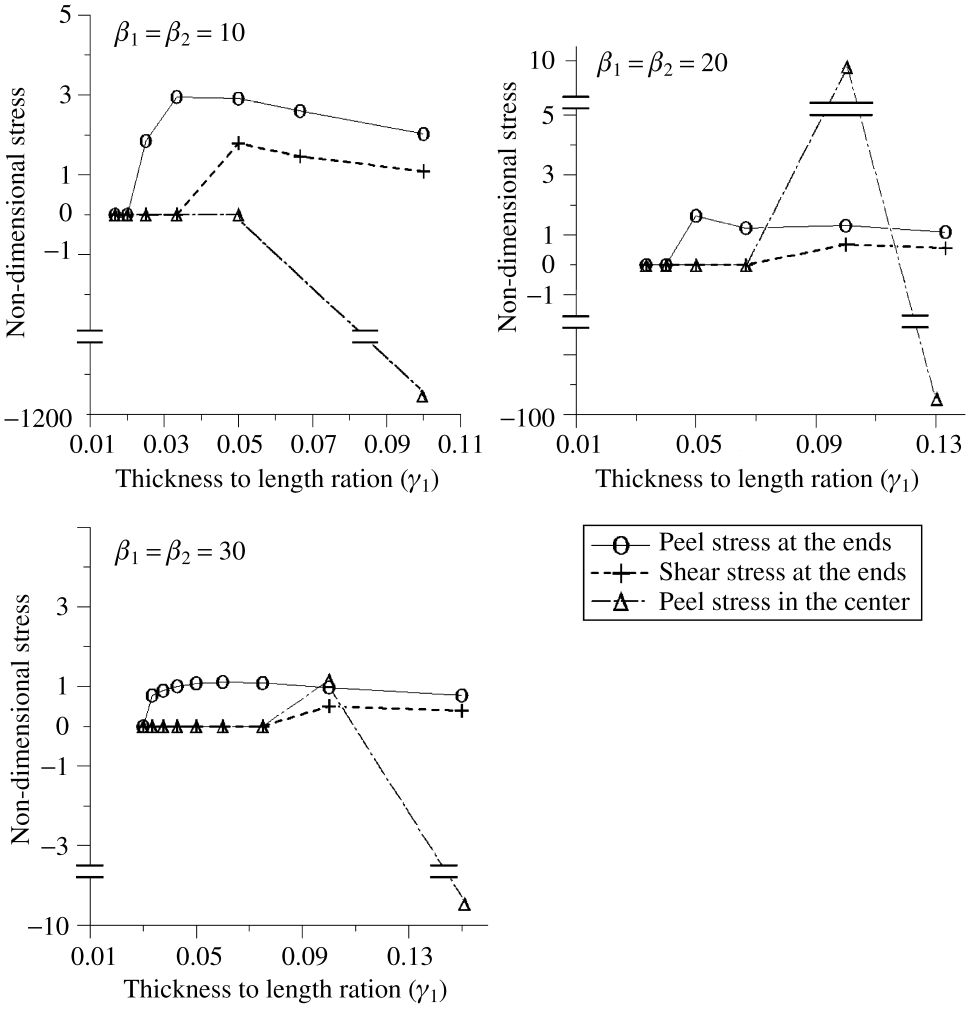

Figure 11. Non-dimensional peel and shear stresses *versus* the thickness to length ratio $\gamma = \gamma_1 = \gamma_2$ for the same thickness of the adherends as for Case 1 ($h_a = 0.01$ mm).

As Fig. 12b indicates, the thickness of the lower adherend is three times that of the lower adherend in Fig. 10, even though otherwise the two figures have the same conditions. However, whether $\gamma_1 = 0.06667$ or $\gamma_1 = 0.01667$, the non-dimensional peel stress vanishes in the center of the adhesive layer. Moreover, the maximum peel stress at the ends of the adhesive layer in Fig. 12b is about one-seventh of that in Fig. 12a, while the maximum shear stress at the ends in Fig. 12b is about one-fifth of that in Fig. 12a.

Figure 13 shows the relationships among non-dimensional peel and shear stresses (at the ends and in the center), as well as the thickness to length ratio γ_1 for the upper adherend: γ_1 is equal to $3\gamma_2$ for Fig. 13a and to $\frac{1}{3}\gamma_2$ for Fig. 13b. The only different condition between Fig. 13a and the top diagram of Fig. 11 is that the thickness

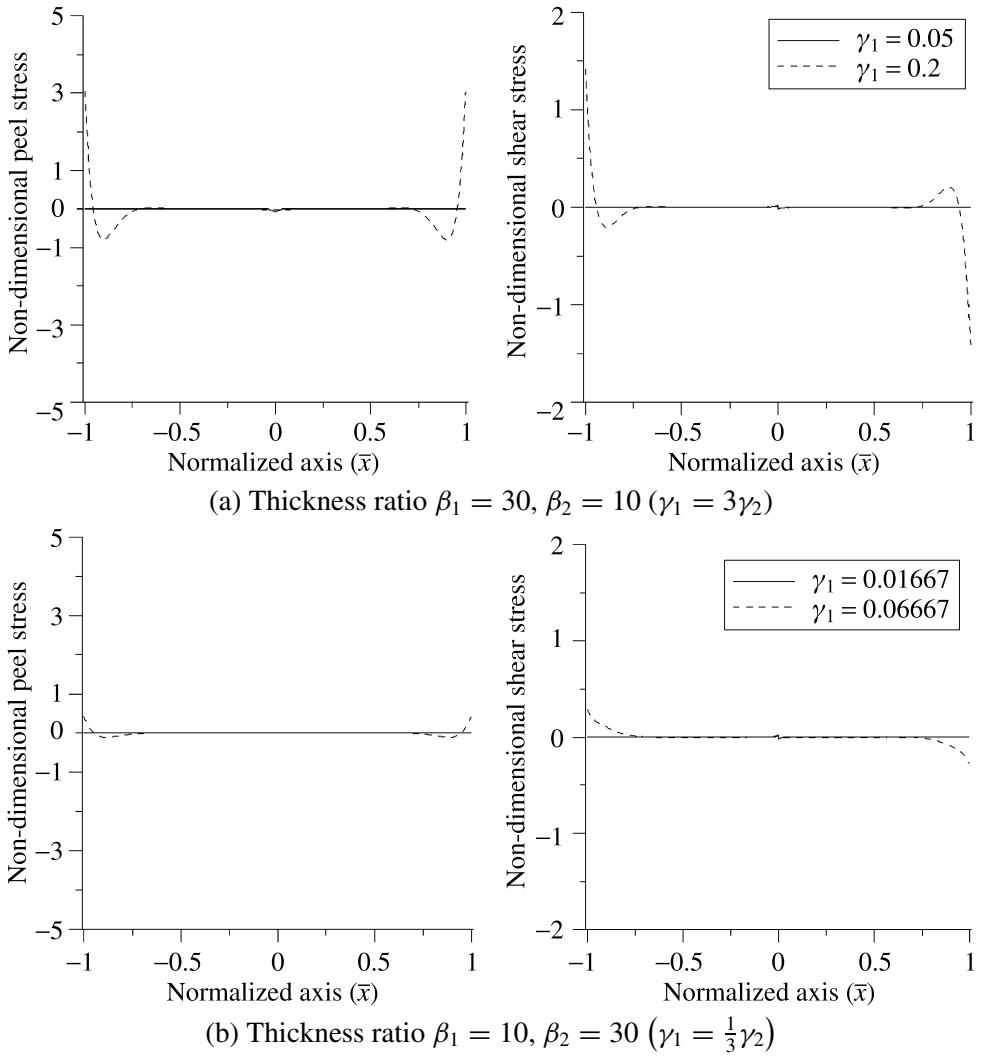

Figure 12. Non-dimensional peel and shear stress distributions in the adhesive layer ($\bar{x} = x/c$) *versus* the thickness to length ratio γ_1 for various thicknesses of the adherends for Case 2 ($h_a = 0.01$ mm).

of the upper adherend in the former is three times that in the latter. However, in Fig. 13a, in contrast to Fig. 11, the compressive peel stress in the center does not occur for γ_1. Consequently, in Fig. 13b the peel stress in the center again vanishes for γ_1 and the maximum peel and shear stresses occur only at the ends. Moreover, whether $\gamma_1 = 3\gamma_2$ or $\gamma_1 = \frac{1}{3}\gamma_2$, the maximum peel and shear stresses for the various lengths of the adhesive layer always occur at the ends. Nevertheless, the maximum peel and shear stresses in Fig. 13a are larger than those in Fig. 13b.

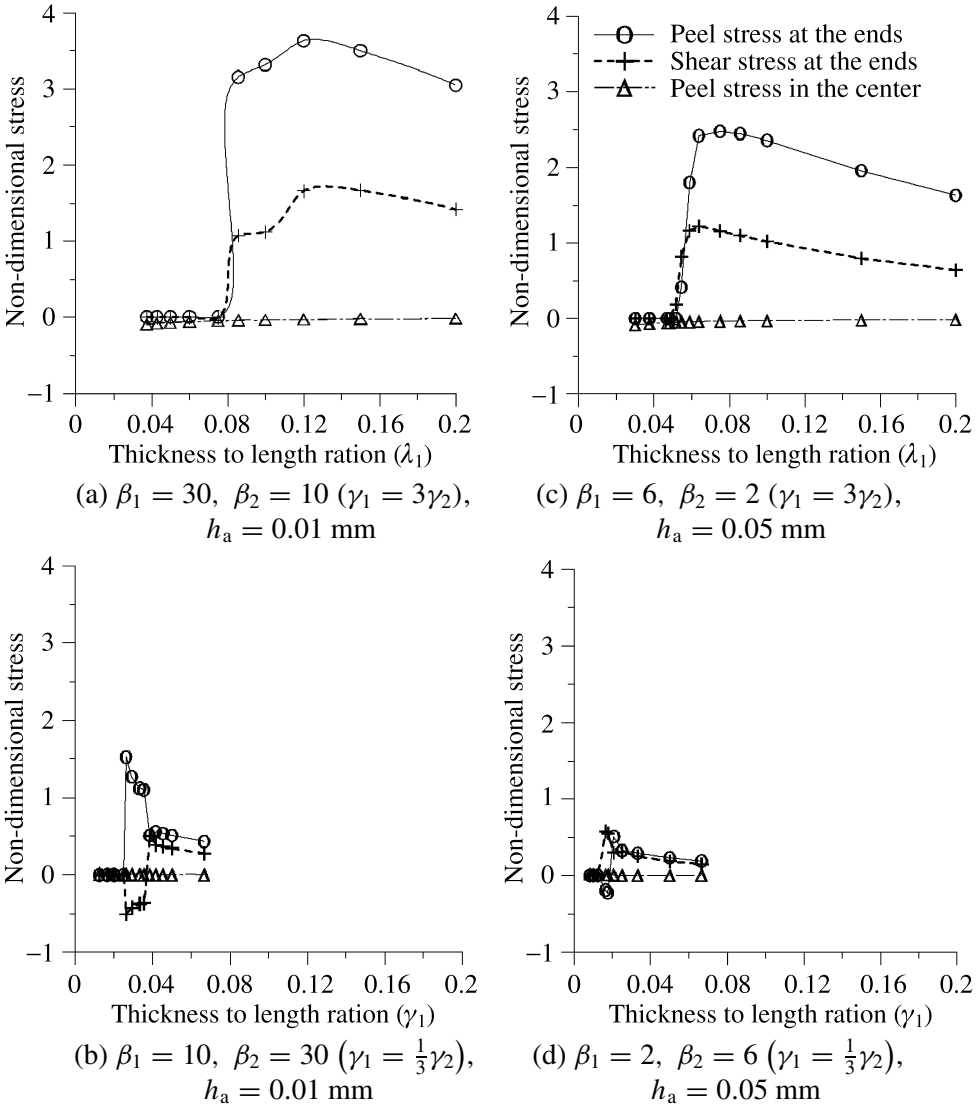

Figure 13. Non-dimensional peel and shear stresses *versus* the thickness to length ratio of the upper adherend γ_1 for various thicknesses of the adherends for Cases 2 and 3.

4.3. Case 3: Adhesive layer with different thickness (h_a)

Comparisons between Fig. 13c and 13d with the $h_a = 0.05$ mm thickness of the adhesive layer and between Fig. 13a and 13b with $h_a = 0.01$ mm adhesive layer thickness are made and described as follows. The only difference between the two sets of figures is the different thickness and the other conditions are the same. Again, the peel stress almost vanishes in the center for Fig. 13a–d, and whether $\gamma_1 = 3\gamma_2$ or $\gamma_1 = \frac{1}{3}\gamma_2$, the maximum peel and shear stresses occur at the ends. The thicknesses $h_a = 0.05$ mm and $h_a = 0.01$ mm of the adhesive layer are compared in Fig.

13a and 13b, and 13c and 13d, respectively. The maximum peel and shear stresses occur at the ends in Fig. 13a–d, but their maximum values in Fig. 13a and 13b ($h_a = 0.01$ mm) are larger than those in Fig. 13c and 13d ($h_a = 0.05$ mm). In Fig. 13a–d, γ_1 values of 0.08, 0.025, 0.05 and 0.015, respectively, begin to bring about the maximum peel and shear stresses at the ends. However, when the adhesive layer is relatively thicker (i.e., $h_a = 0.05$ mm), the thickness to length ratio ($\gamma_1 = 0.05, 0.015$) that begins to bring about the maximum peel and shear stresses at the ends is smaller. That is, the adhesive layer with $h_a = 0.05$ mm thickness may be longer than that with $h_a = 0.01$ mm thickness, but its maximum peel and shear stresses may still occur at the ends.

4.4. Case 4: Action point of force P

As Fig. 14 shows, when $\beta = 10$, $h_a = 0.01$ mm and $\gamma = \gamma_1 = \gamma_2 = 0.01667$, the distributions of the non-dimensional peel and shear stresses are relative to the distance d from the center of the adhesive layer to the action point of force P. Most particularly, the non-dimensional peel and shear stress distributions have a great effect on the distance d for an adhesive layer with a thickness of 0.01mm. However, as Fig. 15 illustrates, when $\beta = 10$, $h_a = 0.02$ mm and $\gamma = \gamma_1 = \gamma_2 = 0.05$, the non-dimensional peel stress distribution has only little effect on the distance d for an adhesive layer with a thickness of 0.02 mm. In Fig. 15, not only does the distribution of the peel stress lead to change in only a small region of the action point, but also it causes virtually no change at the ends. The non-dimensional shear stress at the right end does not change because it is located far from the action point of the force. At the same time, the change in shear stress is due to the action point of the force near the left end.

When the maximum peel stress occurring in the center of the adhesive layer is much larger than the peel and shear stresses at the ends, the upper adherend (IC chip) can easily break. Moreover, according to the preceding results, when both the upper and lower adherends have the same thickness, the adhesive layer is thinner ($h_a = 0.01$ mm), the adherends are thicker and the joint is shorter (i.e., thickness to length ratio $\gamma = \gamma_1 = \gamma_2$ is larger), the adhesively-bonded upper adherend (the IC chip) easily breaks.

Additionally, when the ends and the center of the adhesive layer have small peel and shear stresses, the lower adherend subjected to the concentrated force will also be well joined with the upper adherend. Such joint should be possible under the following conditions: the thickness of the lower adherend is different from that of the upper adherend, and the adhesive layer is thicker and longer. For example, the thicker adhesive layer is 0.05 mm and its length is longer, while the upper and lower adherends are 2- and 6-times thicker than the adhesive layer.

Conversely, the upper adherend (IC chip) without breakage can be completely separated from the lower adherend subjected to the concentrated force when the maximum peel and shear stresses in the adhesive layer at the ends are greater than adhesive criteria stresses. Additionally, when the maximum peel and shear stresses

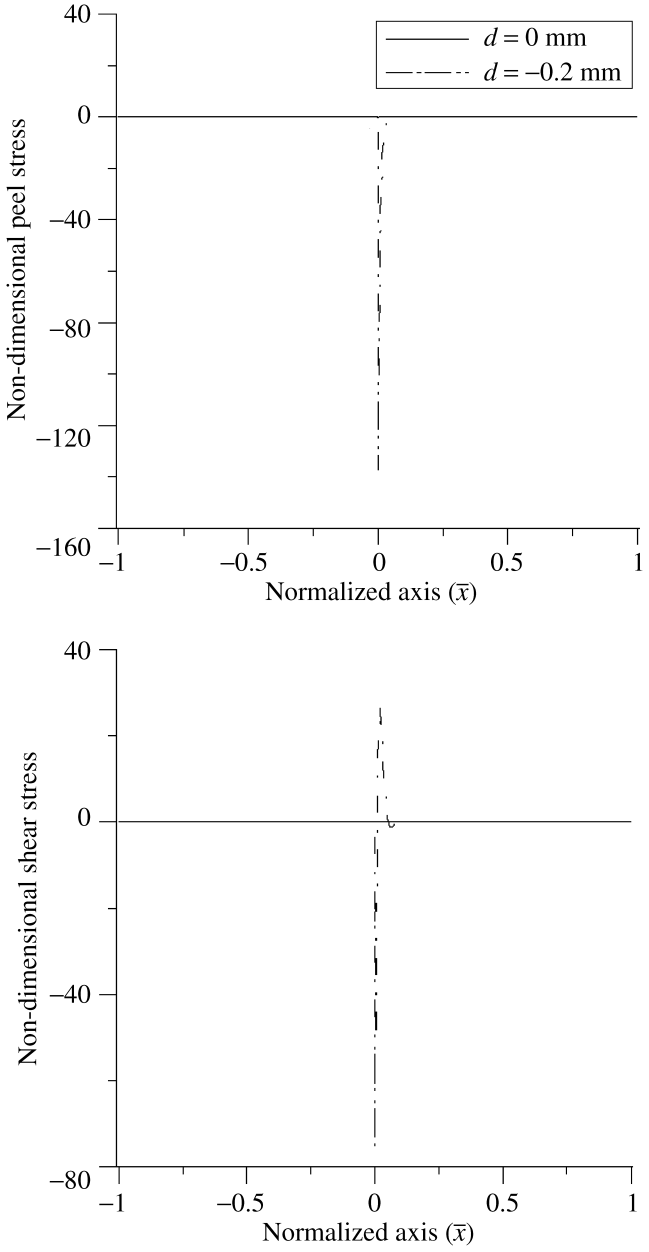

Figure 14. Non-dimensional peel and shear stress distributions for the distance d from the center of the adhesive layer to the action point of the force ($h_a = 0.01$ mm, $\gamma = 0.01667$).

occurring at the ends of the joint are large and the compressive stress in the center of the joint is small, the probability of the upper adherend (IC chip) being easily separated from the lower adherend increases [30]. Thus, the following conditions can satisfy the IC chip pick-up process. The thickness of the lower adherend should

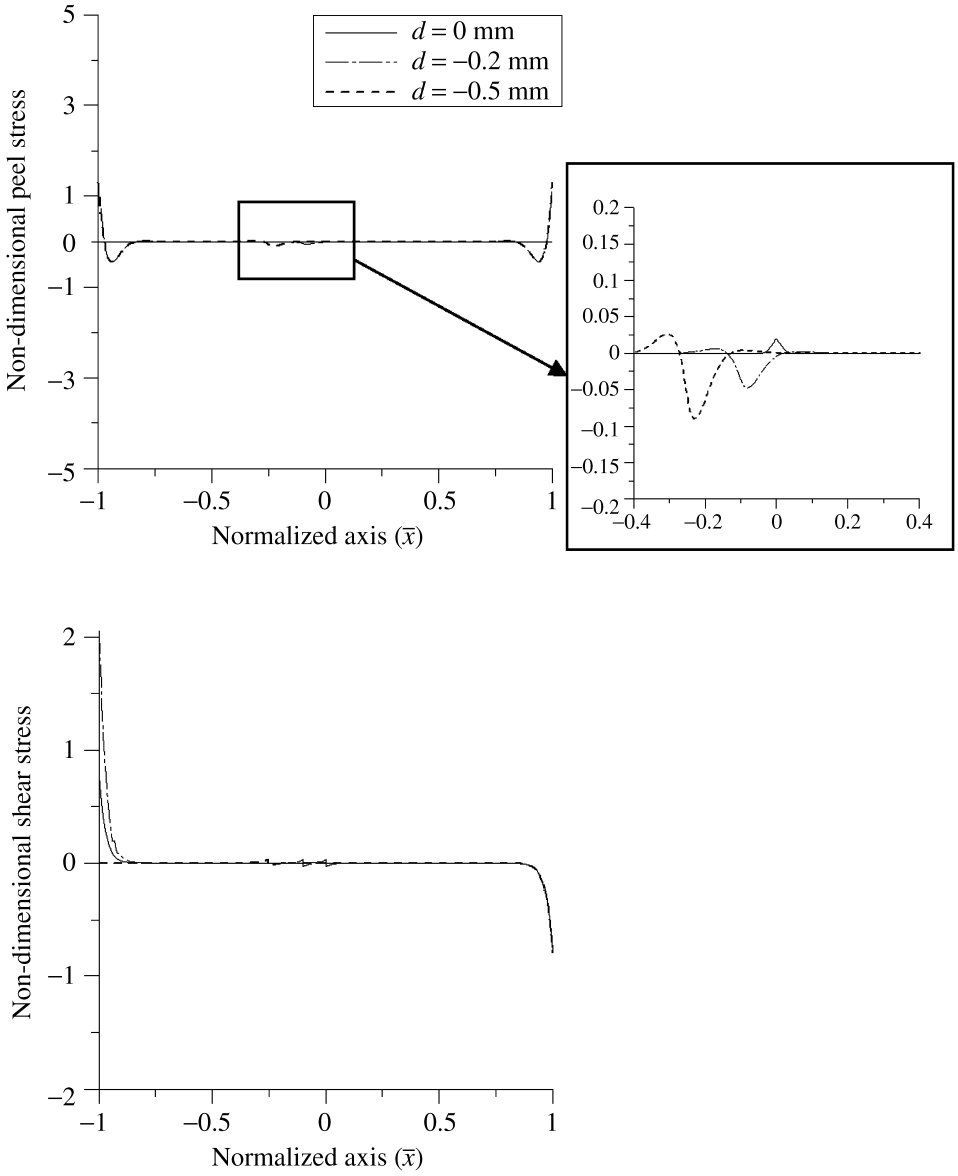

Figure 15. Non-dimensional peel and shear stress distributions for different distances d from the center of the adhesive layer to the action point of force ($h_a = 0.02$ mm, $\gamma = 0.05$).

be greater than ten times that of the adhesive layer but less than one-third that of the upper adherend; and a thin adhesive layer ($h_a \leqslant 0.01$ mm) and a short joint ($\gamma_1 \geqslant 0.08$) should be used.

5. CONCLUSIONS

For two adhesively-bonded adherends, the peel and shear stresses in the adhesive layer are affected by the layer's thickness and length, as well as by the thicknesses of the adherends and the action point of the concentrated force. The complicated coupled equations for this problem were numerically solved using symbolic manipulation and SVD. The maximum peel and shear stresses occurring at the ends of the adhesive layer were analyzed because they dictate whether or not the upper adherend (IC chip) can be separated from the lower adherend. The results indicate that the upper adherend can be completely and easily, separated from the lower adherend under the following conditions: (i) the thickness of the lower adherend should be greater than ten times that of the adhesive layer but less than one-third that of the upper adherend and (ii) the adhesive layer should be relatively thin ($h_a \leqslant 0.01$ mm) and the adhesive joint relatively short (i.e., γ_1 should be greater than 0.08). Thus, the numerical results of this study outline the characteristics of the adhesive layer relative to the adherends, which can be used to develop adhesive joints in the IC chip pick-up process.

Acknowledgements

This project was supported by the National Science Council of R.O.C. under grant number NSC91-2217-E009-012. The authors would like to express their appreciation for the financial support.

REFERENCES

1. M. Goland and E. Reissner, *ASME J. Appl. Mech.* **11**, A17–A27 (1944).
2. D. W. Oplinger, *Int. J. Solids Struct.* **31**, 2565–2587 (1994).
3. W. C. Carpenter, *J. Strain Anal.* **24**, 185–187 (1989).
4. I. U. Ojalvo and H. L. Eidinoff, *AIAA J.* **16**, 204–211 (1978).
5. W. C. Carpenter, *AIAA J.* **18**, 250–352 (1980).
6. T. Wah, *ASME J. Appl. Mech.* **40**, 174–181 (1973).
7. W. J. Renton and J. R. Vinson, *ASME J. Appl. Mech.* **44**, 101–106 (1977).
8. M. Y. Tsai and J. Morton, *Int. J. Solids Struct.* **31**, 2537–2563 (1994).
9. D. J. Allman, *Q. J. Mech. Math.* **30**, 414–436 (1977).
10. Q. Luo and L. Tong, *Int. J. Solids Struct.* **41**, 6351–6381 (2004).
11. A. Özel, M. Aydin and S. Temiz, *J. Adhesion Sci. Technol.* **18**, 313–325 (2004).
12. D. Chen and S. Cheng, *ASME J. Appl. Mech.* **50**, 109–115 (1983).
13. S. Alexandrov and O. Richmond, *Int. J. Solids Struct.* **37**, 669–686 (2000).
14. F. Mortensen and O. T. Thomsen, *Composites Sci. Technol.* **62**, 1011–1031 (2002).
15. E. Suhir, *ASME J. Appl. Mech.* **53**, 657–660 (1986).
16. E. Suhir, *ASME J. Appl. Mech.* **56**, 595–600 (1989).
17. E. Suhir, *Int. J. Solids Struct.* **37**, 2229–2252 (2000).
18. J. N. Rossettos, *J. Adhesion Sci. Technol.* **17**, 115–128 (2003).
19. D. M. Gleich, M. J. L. Van Tooren and A. Beukers, *J. Adhesion Sci. Technol.* **15**, 1247–1259 (2001).
20. P. Qiao and J. Wang, *Int. J. Solids Struct.* **41**, 7423–7444 (2004).

21. Z. Q. Qian and A. R. Akisanya, *Eur. J. Mech. A* **18**, 443–463 (1999).
22. T. Sawa, J. Liu, K. Nakano and J. Tanaka, *J. Adhesion Sci. Technol.* **14**, 43–66 (2000).
23. J. Liu and T. Sawa, *J. Adhesion Sci. Technol.* **14**, 67–92 (2000).
24. J. Lee and H. Kim, *J. Adhesion* **81**, 443–472 (2005).
25. A. Li, T. Assih and Y. Delmas, *J. Adhesion Sci. Technol.* **14**, 1639–1656 (2000).
26. B. Taljsten, *J. Mater. Civil Eng.* **9**, 206–212 (1977).
27. R. W. Cornell, *ASME J. Appl. Mech.* **20**, 355–364 (1953).
28. G. P. Zou, K. Shahin and F. Taheri, *Composite Struct.* **65**, 499–510 (2004).
29. W. H. Press, S. A. Teukolsky, W. T. Vetterling and P. F. Brian, *Numerical Recipes in C*, second edition, pp. 59–70. Cambridge University Press, Cambridge (1992).
30. L. Tong and G. P. Steven, *Analysis and Design of Structural Bonded Joints*. Kluwer Academic Publishers, Dordrecht (1999).